Available online at www.sciencedirect.com
SCIENCE DIRECT®
International Journal of Thermal Sciences 45 (2006) 433–442
International Journal of Thermal Sciences
www.elsevier.com/locate/ijts

Predicted effects of inlet turbulent intensity on mixed convection in vertical tubes with uniform wall heat flux

A. Behzadmehr [a], N. Galanis [b,*], C.T. Nguyen [c]

[a] *Mechanical Engineering Department, University of Sistan & Baluchestan, Iran*
[b] *Génie mécanique, Université de Sherbrooke, QC, Canada J1K 2R1*
[c] *École de génie, Université de Moncton, Moncton, NB, Canada E1A 3E9*

Received 4 August 2004; received in revised form 5 August 2005; accepted 5 August 2005

Available online 5 October 2005

Abstract

Simultaneously developing upward mixed convection of air in vertical tubes with uniform wall heat flux was studied numerically using the three-dimensional elliptic conservation equations. The coupled hydrodynamic and thermal fields were predicted using both laminar and turbulent formulations (the latter was based on the Launder and Sharma low Reynolds number k–ε turbulence model) for $Re = 1000$ and three different values of the inlet turbulent intensity over a wide range of Grashof numbers ($Gr \leqslant 10^8$). The turbulent formulation is more versatile since it can predict turbulent as well as laminar fully-developed flow fields. The effects of inlet turbulent intensity on the axial evolution of the hydrodynamic and thermal fields as well as on the developed velocity and temperature profiles are presented. It is also shown that the increase of the inlet turbulent intensity causes a significant decrease of the wall temperature and of the skin friction coefficient at certain *Re–Gr* combinations.

Keywords: Mixed convection; Developing; Turbulence; Transition; Relaminarization

1. Introduction

Mixed convection in ducts occurs in many industrial installations such as pressurized water reactors, supercritical boilers, solar energy collectors and shell and tube heat exchangers. It is therefore being studied extensively. Jackson et al. [1] presented a comprehensive review of experimental and theoretical studies on mixed convection in vertical tubes published before 1989. Some more recent publications are referred to in the present article.

Numerical studies of mixed convection have been conducted by assuming that the flow field is laminar when *Re* is low or turbulent when *Re* is high. Thus, Wang et al. [2], Nesreddine et al. [3] and Zghal et al. [4] used the laminar equations for $Re < 1500$ while Cotton and Jackson [5], Satake et al. [6], Tanaka et al. [7] used the turbulent equations for $Re > 2000$. Nevertheless, experimental evidence compiled by Metais and Eckert [8] indicates that mixed convection can be turbulent for Reynolds numbers as low as 1000. Furthermore, a flow field which is laminar at the tube entrance may become unstable and eventually turbulent further downstream [9]. Or, as demonstrated by both numerical and experimental studies [6,7,10], a turbulent flow can become laminar under the stabilizing effect of the buoyancy force. It is therefore evident that the laminar model used for the numerical prediction of the corresponding hydrodynamic and thermal fields is of limited practical interest since it can only handle the simplest flow conditions.

Scheele and Hanratty [9] studied experimentally the stability of flow in a vertical tube under mixed convection heat transfer by detecting temperature fluctuations in the effluent. It was found that the stability depends primarily on the shape of the velocity profile and only secondarily on the value of the Reynolds number. Later, Su and Chung [10] analyzed the linear stability of mixed convection flow in a vertical tube. Their results suggest that mixed convection flow in a vertical pipe can become unstable at low Reynolds number and Rayleigh numbers irrespective of the Prandtl number, in contrast to the isothermal case.

* Corresponding author.
E-mail address: nicolas.galanis@usherbrooke.ca (N. Galanis).

1290-0729/$ – see front matter
doi:10.1016/j.ijthermalsci.2005.08.004

Nomenclature

C_f	skin friction coefficient, $= \tau_w/0.5\rho U_0^2$		
C_p	fluid specific heat	$J\cdot kg^{-1}\cdot K^{-1}$	
D	tube internal diameter	m	
g	acceleration of gravity	$m\cdot s^{-2}$	
Gr	Grashof number for isoflux wall, $= g\beta D^4 q_w/\lambda\nu^2$		
Gr_t	Grashof number for isothermal wall, $= g\beta(T_w - T_0)D^3/8\nu^2$		
I	turbulent intensity, $= (2k/3U^2)^{1/2}$		
k	turbulent kinetic energy	$m^2\cdot s^{-2}$	
P	pressure	Pa	
Pr	Prandtl number, $= \mu C_p/\lambda$		
q_w	uniform heat flux at the solid–fluid interface	$W\cdot m^{-2}$	
r	radial coordinate	m	
Re	Reynolds number, $= U_0 D/\nu$		
T, t	time-mean and fluctuating temperature	K	
U, u	time-mean and fluctuating velocity	$m\cdot s^{-1}$	
Z	axial coordinate	m	

Greek letters

β	volumetric expansion coefficient	K^{-1}
ε	dissipation of turbulent kinetic energy	$m^2\cdot s^{-3}$
θ	tangential coordinate	rad
λ	thermal conductivity	$W\cdot m^{-1}\cdot K^{-1}$
μ	dynamic viscosity	$N\cdot s\cdot m^{-2}$
ν	kinematic viscosity	$m^2\cdot s^{-1}$
ρ	density	$kg\cdot m^{-3}$
τ_w	wall shear stress	Pa

Subscripts

b	buoyancy
c	centerline
i, j, k	tensor indexes
w	wall
0	inlet condition
r	radial direction
z	axial direction
θ	tangential direction

In view of this situation, the present research uses a turbulent formulation to study mixed convection with $Re < 2000$. The selected model is the Launder and Sharma low Reynolds number k–ε model [11] which has a proven capability of predicting both laminar and turbulent flows [13,14]. With this approach we have obtained a detailed description of the developing mixed convection flow field in vertical tubes with uniform wall heat flux. Cases with increasing or decreasing turbulence intensity in the flow direction have been presented for $Re = 1000$ [13]. Furthermore we have determined, for $Re = 1000$ and $Re = 1500$, the critical Grashof numbers which correspond to laminar-turbulent transition and relaminarization of the flow as well as the Re–Gr combination that result in a pressure decrease over the tube length from those resulting in a pressure increase [14].

In the present paper, we show new results for ascending mixed convection of air in a vertical tube with uniform wall heat flux and $Re = 1000$ calculated numerically from the selected low Reynolds number k–ε model. In particular, we present the effects of turbulent intensity at the tube inlet on the hydrodynamic and thermal fields, on the critical Grashof number and on the skin friction coefficient.

2. Mathematical formulation, numerical procedure and validation

We consider steady state upward flow in a long vertical tube with uniform heat flux at the fluid–solid interface. The properties of the fluid are assumed constant except for the density in the body force, which varies linearly with temperature (Boussinesq's hypothesis) as in many previous studies [4,5,7]. Dissipation and pressure work are neglected as in all the previous numerical studies mentioned in the introduction. With these assumptions the dimensional conservation equations for steady state mean conditions are as follows:

$$\frac{\partial U_j}{\partial X_j} = 0 \tag{1}$$

$$\rho\frac{\partial}{\partial X_j}(U_j U_i) = -\frac{\partial P}{\partial X_i} + \frac{\partial}{\partial X_j}\left[\mu\left(\frac{\partial U_i}{\partial X_j} + \frac{\partial U_j}{\partial X_j}\right) - \rho\overline{u_i u_j}\right] + \left[1 + \beta(T - T_0)\right]\rho g_i \tag{2}$$

$$\rho\frac{\partial}{\partial X_j}\left(C_p U_j \frac{\partial T}{\partial X_j}\right) = \frac{\partial}{\partial X_j}\left[\lambda\frac{\partial T}{\partial X_j} - C_p\rho\overline{u_j t}\right] \tag{3}$$

In cylindrical coordinates

$$X_1 = r, \qquad X_2 = \theta, \qquad X_3 = Z \tag{4a}$$

while for Z positive in the flow direction:

$$g_1 = g_2 = 0 \quad \text{and} \quad g_3 = -g \tag{4b}$$

Turbulence is modeled using the Launder and Sharma [11] low Reynolds number k–ε model. This has been shown by Patel et al. [15] and Mikielewicz et al. [16] to be appropriate for the study of mixed convection. It is expressed by the following equations:

$$\frac{\partial}{\partial X_j}(U_j k) = \frac{\partial}{\partial X_j}\left[\left(\nu + \frac{\nu_t}{\sigma_k}\right)\frac{\partial K}{\partial X_j}\right] + G_k + G_b - \varepsilon - 2\nu\left(\frac{\partial\sqrt{k}}{\partial X_j}\right)^2 \tag{5}$$

$$\frac{\partial}{\partial X_j}(U_j \varepsilon) = \frac{\partial}{\partial X_j}\left[\left(\nu + \frac{\nu_t}{\sigma_\varepsilon}\right)\frac{\partial \varepsilon}{\partial X_j}\right] + c_1 f_1\frac{\varepsilon}{k}(G_k + G_b) - c_2 f_2\frac{\varepsilon^2}{k} + E \tag{6}$$

where

$$G_k = -\overline{u_i u_j}\frac{\partial U_i}{\partial X_j}, \qquad G_b = -\frac{\beta}{\rho} g_i \overline{u_i t} = g_i \frac{\beta}{\rho}\frac{\nu_t}{Pr_t}\frac{\partial T}{\partial X_i}$$

$$\nu_t = c_\mu f_\mu \frac{k^2}{\varepsilon}, \qquad c_1 = 1.44, \qquad c_2 = 1.92$$

$$c_\mu = 0.09, \qquad f_1 = 1, \qquad Pr_t = 0.9$$

$$\sigma_k = 1, \qquad \sigma_\varepsilon = 1.3, \qquad R_t = \frac{k^2}{\nu\varepsilon}$$

$$f_2 = 1 - 0.3\exp\left(-R_t^2\right), \qquad f_\mu = \exp\left[\frac{-3.4}{(1 + R_t/50)^2}\right]$$

$$E = 2\nu\nu_t\left(\frac{\partial^2 U_i}{\partial X_j \partial X_k}\right)^2 \tag{7}$$

These equations have been presented in cylindrical coordinates with the boundary layer approximation [5] and for fully developed flow [7]. The present study does not use any of these simplifications.

This set of coupled, elliptical non-linear differential equations was discretized with the control volume technique. For the convective and diffusive terms a second order upwind method was used while the SIMPLEC procedure was introduced for the velocity-pressure coupling. The discretization grid was uniform in the circumferential direction and non-uniform in the other two directions. It was finer near the tube entrance and near the wall where the velocity and temperature gradients are large. The solution was obtained using the following boundary condition:

- at the tube entrance ($Z = 0$):

$$U_z = U_0, \qquad U_\theta = U_r = 0, \qquad T = T_0, \qquad I = I_0 \tag{8a}$$

Since the adopted model incorporates the assumption of turbulence isotropy, the corresponding turbulent kinetic energy is:

$$k_0 = 1.5(I_0 U_0)^2 \tag{8b}$$

- at the tube outlet ($Z/D = 98$) the diffusion flux in the direction normal to the exit plane is assumed to be zero for all variables and an overall mass balance correction is applied [19].
- at the fluid–solid interface ($r = D/2$)

$$U_r = U_\theta = U_Z = 0, \qquad k = \varepsilon = 0, \qquad q_w = -\lambda\frac{\partial T}{\partial r} \tag{9}$$

Several different grid distributions have been tested to ensure that the calculation results are grid independent. The selected grid consists of 220, 48 and 8 nodes respectively in the axial, radial and circumferential directions.

In order to validate the turbulent formulation and the numerical procedure, the predicted velocity and temperature profiles were compared with experimental results for two very different conditions. Thus, for developing flow in a vertical isothermal tube with $Re = 379.8$, $Gr = 12628$, the numerical results for $I_0 = 0.1\%$ and $I_0 = 8\%$ at $Z/D = 5.5$ and $Z/D = 62.4$ agree very well with the measured values [17] as shown in Fig. 1. It is important to notice that the imposed inlet turbulence has no significant effect on the velocity profile even quite close to the tube entrance ($Z/D = 5.5$). The agreement between the corresponding predicted and experimental temperature profiles, which are not presented here for lack of space, is equally good. Furthermore, the adopted turbulent formulation predicts that, in this case, the turbulent kinetic energy tends to zero as Z is increased. Thus, for these conditions, the model correctly predicts that the flow beyond the entry region is laminar. Additionally, the numerically predicted velocity and temperature profiles for fully developed conditions with $Re = 1000$ and two different Grashof numbers have been shown [14] to be in excellent agreement with Hallman's [20] analytical results for laminar mixed convection. These comparisons indicate that the adopted turbulent formulation can satisfactorily predict both developing and fully developed laminar mixed convection. Finally, the predicted velocity and temperature profiles were compared with experimental results by Carr et al. [18] corresponding to fully developed turbulent flow ($Re = 5000$, $Gr = 2.22 \times 10^7$). As shown previously [13,14] the measured and calculated profiles are in very good agreement. Furthermore, for these conditions, the calculated turbulent kinetic energy at the tube outlet is important, indicating that the model correctly predicts a turbulent flow.

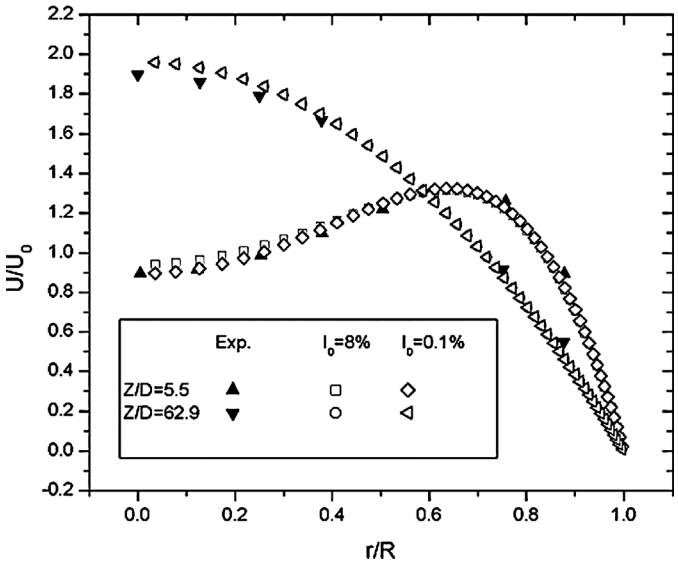

Fig. 1. Validation for $Re = 379.8$, $Gr_t = 12628$ [17] and two different values of the inlet turbulent intensity.

These numerical tests and observations indicate that the adopted turbulent formulation can be used to study both laminar and turbulent mixed convection flows. To the knowledge of the authors, this is the first time that this capability of the low Reynolds number k–ε model has been observed.

3. Results and discussion

The results presented here were calculated with $Pr = 0.71$, $L = 98D$, $Re = 1000$ for three different values of I_0 (0.1%, 1%, 8%) and a wide range of Grashof numbers ($Gr \leqslant 10^8$). Similar results were obtained for $Re = 1500$ and other values of I_0 but are not presented here for lack of space. It should be noted that for all combinations of Re and I_0 investigated here, all the calculated variables (U, T, C_f, k, ε, ...) tend towards axially

independent values as the flow moves downstream from the inlet. This observation confirms the existence of a fully developed region as argued earlier [13].

3.1. Effect of inlet turbulent intensity on the flow regime

Fig. 2 shows the predicted axial evolution of the turbulent kinetic energy at the tube axis for three different inlet turbulent intensities and four Grashof numbers. Radial distributions of k at different axial positions have also been obtained but are not shown here because of space limitations. For the lowest Grashof number ($Gr = 7.1 \times 10^5$, Fig. 2(a)) in the case of $I_0 = 0.1\%$, and $I_0 = 1\%$ the inlet turbulent kinetic energy is damped monotonically to zero as the fluid moves downstream. The corresponding fully developed flow fields are therefore laminar. On the other hand, for $I_0 = 8\%$ the turbulent kinetic energy at first decreases and then increases towards an important asymptotic value. The decrease immediately after the inlet is caused by the increase of the centerline velocity due to boundary layer growth in the entrance region where thermal effects are negligible. The subsequent growth of k_c is due to the simultaneous increase of buoyancy and thermal turbulent production and of turbulent diffusion. For this combination of parameters ($Gr = 7.1 \times 10^5$, $I_0 = 8\%$) the fully developed flow is turbulent. When the Grashof number increases to 8×10^6 (Fig. 2(b)) the inlet turbulent kinetic energy is damped to zero for $I_0 = 0.1\%$ only. For the other two values of I_0, k_c increases suddenly and reaches a local maximum value at $Z/D \cong 12$ and $Z/D \cong 9$, respectively for $I_0 = 1\%$ and $I_0 = 8\%$. Beyond this point, it is damped towards a constant non-zero value which indicates a turbulent fully developed flow regime. The local maximum is higher for the lower inlet intensity ($I_0 = 1\%$) because of a higher turbulent production as will be explained later by analyzing the velocity profiles.

Similar behaviors are observed for $Gr = 3 \times 10^7$ (Fig. 2(c)). The corresponding increase of the wall heat flux causes higher near wall buoyancy forces and consequently higher near wall velocity gradients. Therefore, the turbulent kinetic energy increases earlier than in Fig. 2(b). In the present case, local maxima are observed for all values of I_0. They occur at $Z/D \cong 10$, $Z/D \cong 8$ and $Z/D \cong 6$ respectively for $I_0 = 0.1\%$, $I_0 = 1\%$ and $I_0 = 8\%$. Furthermore, the constant asymptotic values of k_c are non-zero for all three values of I_0 indicating that for this Grashof number the corresponding fully developed flow

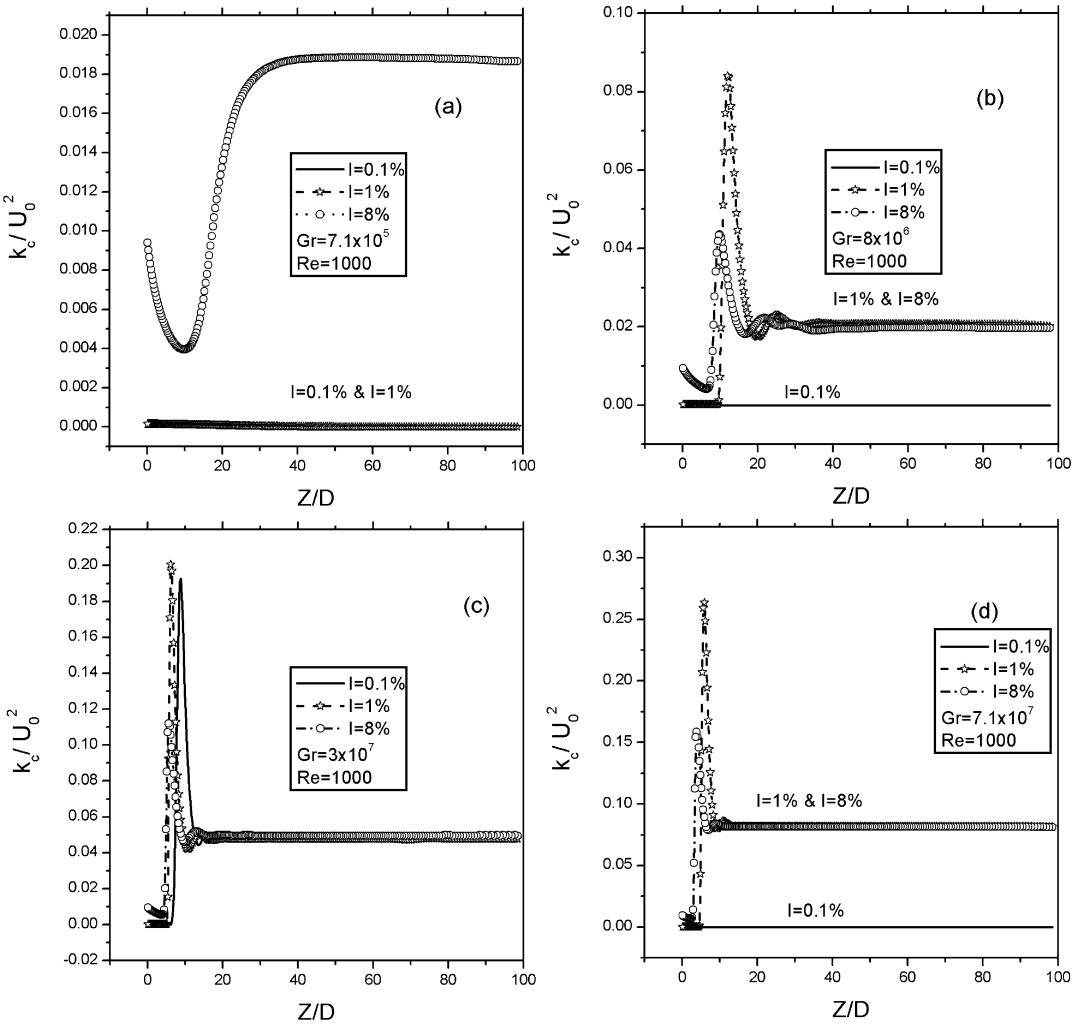

Fig. 2. Axial variation of turbulent kinetic energy at the centerline.

regimes are all turbulent. Finally, for $Gr = 7.1 \times 10^7$ (Fig. 2(d)), k_c is damped to zero for the lowest inlet turbulent intensity, $I_0 = 0.1\%$, while it increases to a local maximum and is then damped to a non-zero constant value for the other two inlet turbulent intensities. These non-zero constant values for $I_0 = 1\%$ and $I_0 = 8\%$ show that the corresponding flow field are still turbulent. On the other hand, for the lowest inlet turbulent intensity, $I_0 = 0.1\%$, the fully developed flow field is no longer turbulent because of the stabilizing effect of the near wall acceleration caused by the buoyancy forces [13]. This relaminarization has also been observed for accelerating flows in converging passages [12].

These results indicate that the flow regime in the fully developed region depends on the values of both Gr and I_0. Thus, for $I_0 = 0.1\%$ the fully developed flow field is laminar for low and high value of Gr. The transition from laminar to turbulent regime occurs at a critical Grashof number between 9×10^6 and 1×10^7 while the relaminarization occurs at a second critical Grashof number between 5×10^7 and 7.1×10^7. For $I_0 = 1\%$ the first critical Grashof number is between 8×10^5 and 1×10^6 while the second one is higher than 7.1×10^7. In general, as I_0 increases the first critical value of Gr decreases since lower buoyancy turbulent production is needed to change the flow field from laminar to turbulent. On the other hand, the second critical value of Gr increases as I_0 increases because a higher near-wall velocity is needed to stabilize the flow field under these conditions.

Fig. 2, also shows that, for a fixed value of I_0, the local maximum of k_c moves towards the tube inlet when the Grashof number increases. For a fixed value of Gr, this maximum occurs sooner for the higher values of I_0. All of these observations are a result of the combined effects of the buoyancy turbulent production (term G_b in Eq. (5)) which interacts with the inlet turbulence. This effect of the inlet turbulence on the flow regime in the fully developed region cannot be predicted by linear stability analysis such as the study by Su and Chung [10].

3.2. Prediction and analysis of the velocity field

Fig. 3 shows the evolution of the centerline axial velocity along the tube length. For the lowest Grashof number ($Gr = 7.1 \times 10^5$, Fig. 3(a)), U_c initially increases from its inlet value ($U = U_0$) as the boundary layer builds up and pushes the fluid

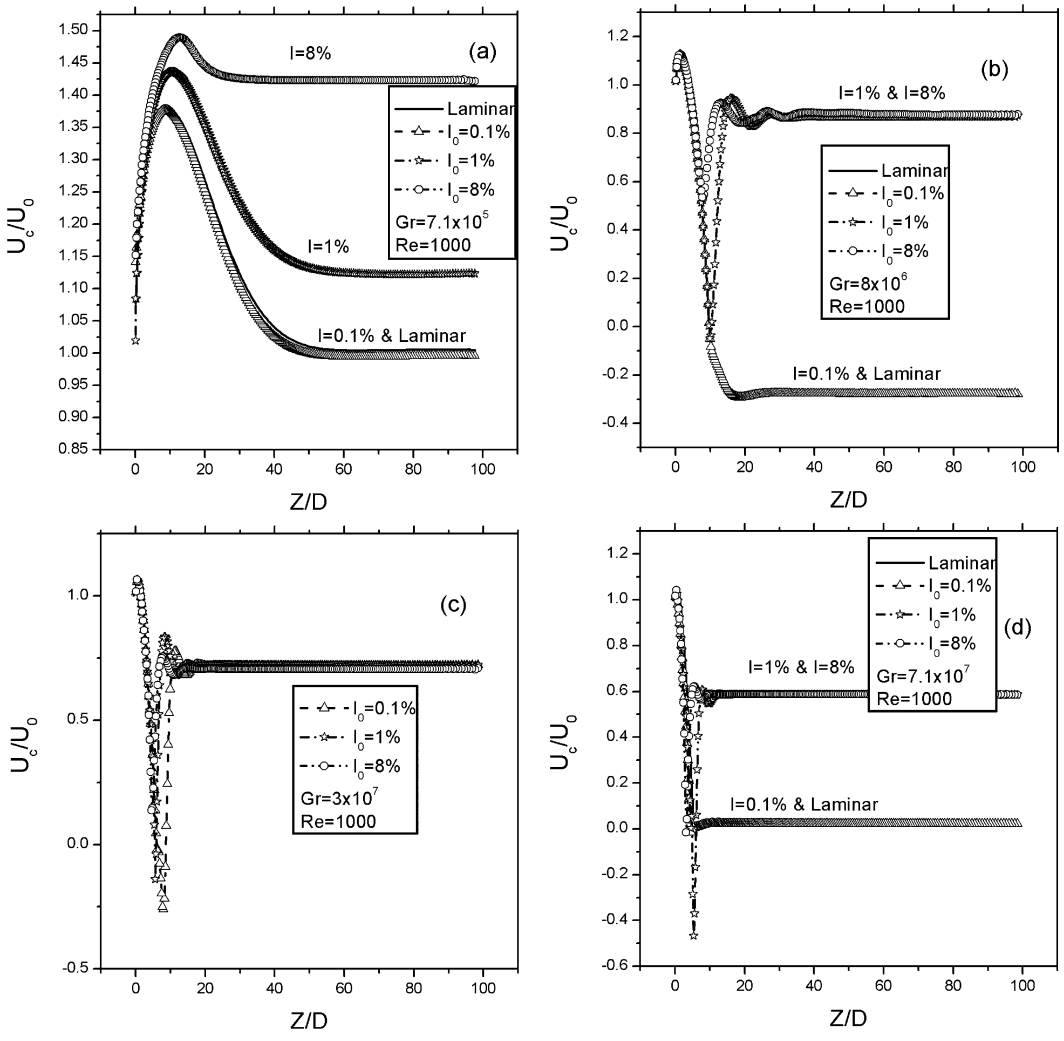

Fig. 3. Axial variation of centerline axial velocity.

towards the tube axis. It reaches a maximum value which increases as I_0 increases. Then, as the near wall upward buoyancy force increases, the fluid near the wall accelerates and, consequently, the velocity in the centerline region decreases to respect continuity. In the case of $I_0 = 8\%$, since the flow regime is turbulent (cf. Fig. 2(a)) and radial momentum diffusion is important, this decrease of U_c is small compared to the three other cases (laminar, $I_0 = 0.1\%$ and $I_0 = 1\%$). It is interesting to note that the predictions of the turbulent model with $I_0 = 0.1\%$ are essentially identical with those of the laminar formulation obtained by setting $\overline{u_i u_j} = \overline{u_j t} = 0$ in Eqs. (2) and (3). As mentioned earlier the laminar fully developed numerical profiles are in very close agreement with the analytical solution by Hallman [20]. On the other hand, in the case of $I_0 = 1\%$ the axial evolution of U_c is different from the previous two even though all three are laminar in the fully developed region (cf. Fig. 2(a)). This residual influence of the inlet turbulent intensity on the three laminar fully developed profiles is illustrated in Fig. 4(a). We notice that the profile predicted by the laminar model and by the turbulent model with $I_0 = 0.1\%$ are essentially identical while the one for $I_0 = 1\%$ is decidedly different. The maximum velocity for these three cases occurs far from the axis, a situation characteristic of laminar mixed convection [3,4]. On the other hand, for $I_0 = 8\%$ the maximum velocity occurs at the tube axis as expected for turbulent flows.

Analogous results are shown in Figs. 3(b) and 4(b) for $Gr = 8 \times 10^6$. In this case however, the maximum value of U_c does not depend on I_0. It occurs earlier and is smaller than in the previous case since the near wall acceleration caused by buoyancy is more important due to the higher value of the wall heat flux. The value of U_c predicted by the turbulent model with $I_0 = 0.1\%$ and by the laminar model are identical. Downstream from the position of the maximum, the value of U_c for these two cases decreases monotonically and reaches a negative asymptotic value which indicates the existence of flow reversal at the axis. Fig. 4(b) shows that the region of flow reversal extends approximately to $r/D \cong 0.2$. It also shows that the maximum velocity is greater and occurs closer to the wall than for $Gr = 7.1 \times 10^5$. It is again noted that all these laminar fully developed profiles have been shown to agree very well with the corresponding analytical solution [20]. For $I_0 = 1\%$ and $I_0 = 8\%$, downstream from the position of the maximum, U_c decreases for a while as the effects of wall heating cause an upward acceleration in the region near the wall. However, when turbulent production due to hydrodynamic and thermal effects increases (see Fig. 2(b) for Z/D between 10 and 20), radial diffusion of momentum increases and results in an increase of U_c. In the fully developed region, the values of U_c for these two turbulent flows are the same. In fact, as shown in Fig. 4(b), the entire fully developed velocity profiles for these two cases are identical.

It is now possible to explain why the maximum centerline turbulent kinetic energy in Fig. 2(b) is higher for $I_0 = 1\%$ than for $I_0 = 8\%$. As indicated by the results in Figs. 2 and 3 (as well as by other more detailed result not shown here for lack of space) the region immediately after the tube inlet in which U_c increases and k_c decreases due to boundary layer growth

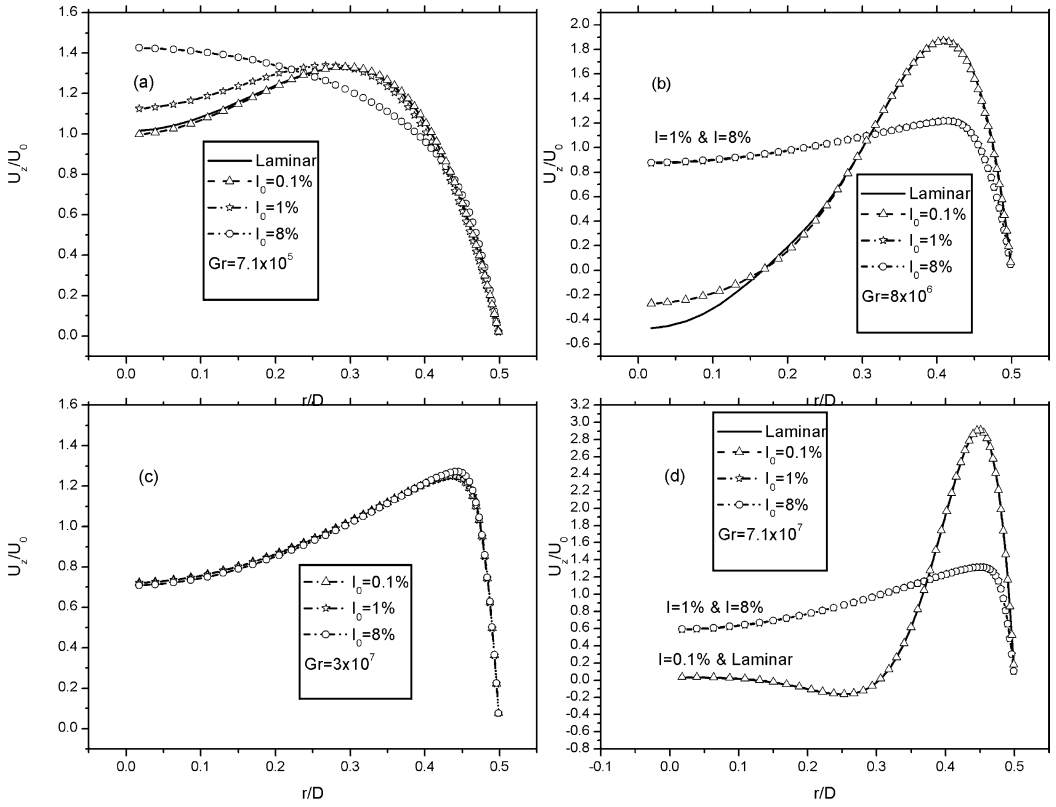

Fig. 4. Fully developed velocity profiles.

(a hydrodynamic effect influenced by the Reynolds number) is followed by a second region in which thermal effects are significant: the ensuing acceleration of the fluid near the wall causes a decrease of U_c and an increase of k_c. The axial gradient of U_c constitutes a local source of turbulence. Furthermore, the significant velocity and temperature gradients in the boundary layer constitute additional sources of turbulence which diffuses towards the centerline. For a given Grashof number, these gradients increase with Z but are essentially independent of I_0. These turbulence sources combine with the local residual of the inlet turbulence to trigger the sudden increase of k illustrated in Fig. 2. Since at any given axial position, the turbulence sources caused by the velocity and temperature gradients are the same for $I_0 = 1\%$ and $I_0 = 8\%$ while the local residual of the inlet turbulence is higher for $I_0 = 8\%$, the increase of k occurs earlier in the latter case. Therefore, at the position where the increase of k takes place, the velocity and temperature gradients are more important for $I_0 = 1\%$ and thus the increase of k is more significant.

Fig. 3(c) shows the evolution of the centerline axial velocity along the tube length for $Gr = 3 \times 10^7$. As indicated by the results in Fig. 2(c), the fully developed flow field is in this case turbulent for the three values of I_0 under consideration. Significantly, for this Grashof number the laminar model did not converge despite several attempts with different discretizations and different relaxation schemes. In all cases, the local values of the calculated variables were unstable similarly to experimental results [21]. This behavior confirms the limitation of the steady laminar model. It is interesting to note in Figs. 3(c) and 4(c) that the corresponding velocities in the region $0 \leqslant Z/D < 6$ and $17 \leqslant Z/D \leqslant 98$ are identical for the three different values of I_0. It is also important to note in Figs. 3(b), 3(c) and 3(d) the presence of a short region with flow reversal which occurs very close to the tube inlet.

The variation of U_c along the tube length for the highest Grashof number is shown in Fig. 3(d) while the corresponding fully developed velocity profiles are shown in Fig. 4(d). The turbulent results for $I_0 = 0.1\%$ are essentially identical with the corresponding predictions from the laminar model. This observation is consistent with the evolution of k_c for $I_0 = 0.1\%$ shown in Fig. 2(d). In this case flow reversal occurs in the fully developed region at a position which does not include the tube axis (see Fig. 4(d)). The maximum velocity occurs very close to the wall (at $r/D \cong 0.45$) and is very high ($U/U_0 \cong 3$). These results are identical to those predicted by the corresponding analytical solution [20]. On the other hand, for $I_0 = 1\%$ and $I_0 = 8\%$ the fully developed flow is turbulent (see Fig. 2(d)) and the corresponding velocity profiles are indistinguishable (Fig. 4(d)). However, in the inlet region the evolution of U_c is quite different for these two inlet turbulence intensities. In particular, for $I_0 = 1\%$ flow reversal centered at the tube axis is observed over a very short distance at about the same axial position where the corresponding sudden increase of k_c takes place (cf. Fig. 2(d)).

3.3. Axial evolution of the skin friction coefficient

Fig. 5 shows the evolution of the non-dimensional skin friction coefficient along the tube length. At $Z = 0$ the value of C_f is the same for all Grashof numbers and it initially decreases since natural convection effects do not become effective immediately at the tube entrance. This is qualitatively consistent to the corresponding behaviour for flow over a flat plate. As the Gr increases the length of this region decreases since the effects of heating become more pronounced. For the lowest Grashof number ($Gr = 7.1 \times 10^5$), Fig. 4(a), C_f reaches a local minimum at approximately $Z/D = 5$, increases slightly and attains a constant value in the hydrodynamically developed region. This behaviour has been noted previously for laminar mixed convection [3,4] but not for turbulent mixed convection. The values for the laminar prediction and the turbulent prediction with $I_0 = 0.1\%$ are the same (approximately 0.03) while for the higher turbulent intensities the fully developed values are higher (approximately 0.034 for $I_0 = 1\%$, and 0.038 for $I_0 = 8\%$). For $Gr = 8 \times 10^6$, in the cases of the laminar formulation and the turbulent one with $I_0 = 0.1\%$, C_f increases after the entry region, reaches a local maximum and attains a constant value of approximately 0.09 in the fully developed region. It is noted that, according to the previous discussion, the developed flow for these two cases is laminar. In the cases of $I_0 = 1\%$ and $I_0 = 8\%$ also, for which the fully developed flow is turbulent, the variation of C_f is qualitatively the same as for the two previous cases. However, both the local maximum and the fully developed values of C_f are higher for the two cases corresponding to laminar fully developed flow. By comparing the values of C_f for the three different inlet intensities, it is found that both its local maximum and its fully developed values decrease as I_0 increases. This behaviour is due to the fact that a higher turbulent intensity increases the radial momentum diffusion and results in a more uniform velocity profile (see Fig. 4(b)). On the other hand, in the case of laminar flow the near wall buoyancy force increases the fluid velocity in this region (see Fig. 4(b)) and results in very high shear stress at the solid–fluid interface.

For $Gr = 3 \times 10^7$, for which the fully developed flow is turbulent for all three inlet turbulent intensities, we note a pronounced peak corresponding to the position of minimum U_c (cf. Fig. 3(c)) and steeply increasing k_c (cf. Fig. 2(c)). The fully developed value of C_f is slightly higher for the highest I_0. Finally, for $Gr = 7.1 \times 10^7$ the values of C_f are much higher than those for all previous cases. The qualitative behaviour is the same as that for $Gr = 8 \times 10^6$ (see Fig. 4(b)). It should be noted that the value of C_f for hydrodynamically developed forced convection is 0.016, i.e. considerably smaller than all the corresponding values shown in Fig. 5.

3.4. Presentation and analysis of the temperature field

Fig. 6(a) shows the axial evolution of the non-dimensional wall temperature for $Gr = 7.1 \times 10^5$. Immediately after the tube inlet, the rate of increase of T_w is very high (consistently with experimental results [9]) and its value is independent of I_0. At

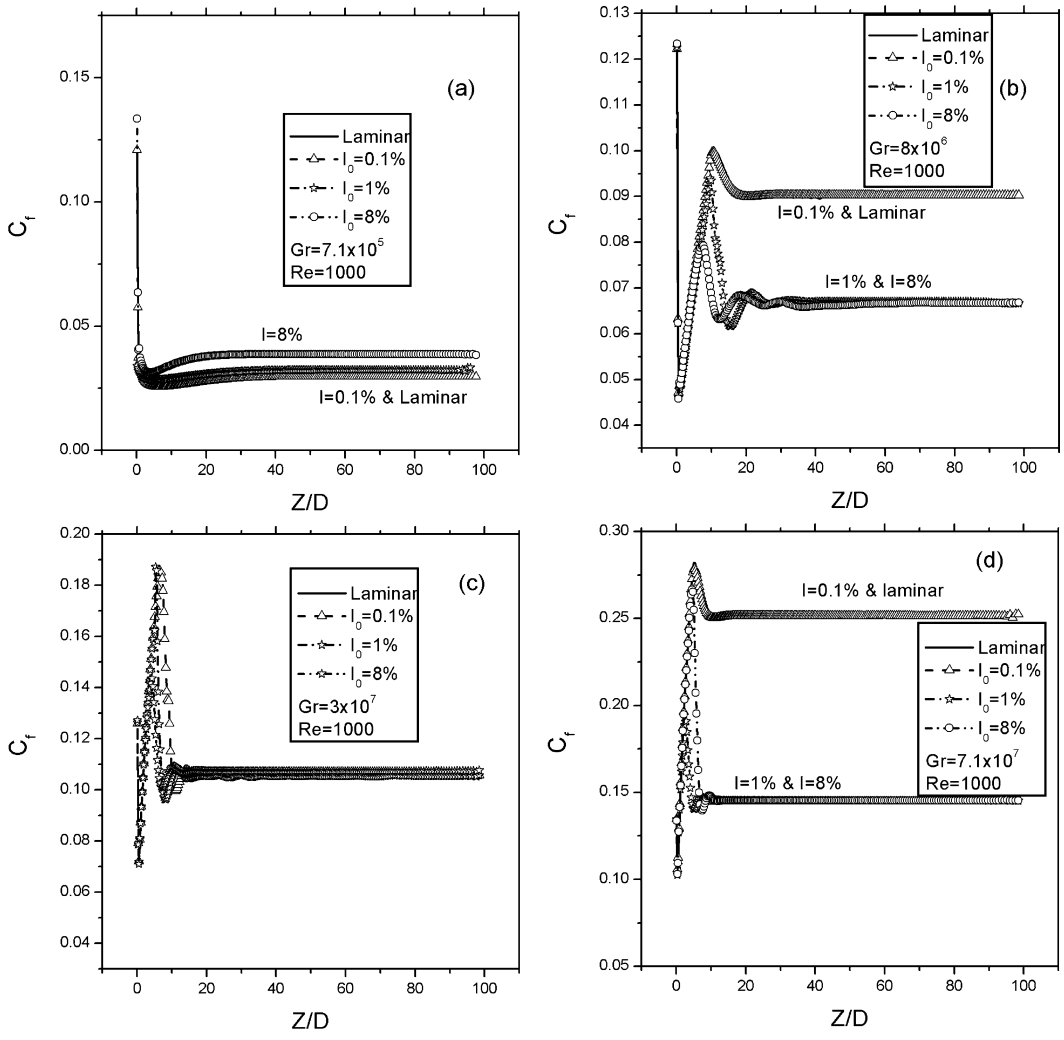

Fig. 5. Axial variation of the skin friction coefficient.

$Z/D \cong 5$, i.e. very close to the position where the centerline velocity becomes dependent on I_0 (see Fig. 3(a)) and C_f is minimum (see Fig. 5) the slope of T_w for $I_0 = 8\%$ changes significantly from that of the other three cases (laminar, $I_0 = 0.1\%$ and $I_0 = 1\%$). In fact, the wall temperature for the latter three cases is almost identical over the entire length of the tube.

Its axial evolution is qualitatively similar to the corresponding results by Scheele and Hanratty [9]. On the other hand, the wall temperature for $I_0 = 8\%$ is, at any axial position beyond $Z/D \cong 5$, significantly lower than that for the other three cases. We note that the wall heat flux is the same for all four cases in Fig. 6(a) while the flow field is turbulent for $I_0 = 8\%$ and laminar for the other two inlet intensities (see Fig. 2(a)). Therefore, the results of Fig. 6(a) indicate that it is possible to maintain the wall at a low temperature, without increasing the mass flow rate or decreasing the heat flux, by simply increasing the turbulence of the flow at the inlet of the tube. This effect is particularly interesting for the cooling of gas-cooled nuclear reactors.

Beyond $Z/D \cong 20$ the wall temperatures in Fig. 5(a) increase linearly with axial distance. The slope of this line is approximately 0.0059 which is very close to the corresponding non-dimensional gradient of the fluid bulk temperature calculated by applying the first law of thermodynamics to the fluid within the tube. Because of the choice of the reference temperature used to non-dimensionalize the difference $(T_w - T_0)$, this slope is inversely proportional to the Peclet number (which is constant for all the cases considered in this study) and independent of the Grashof number. Thus, the wall temperature trends for the other three Grashof numbers quoted in the previous figures are quite similar to those in Fig. 6(a) and are not presented here. The only notable differences are:

- the length of the entry region, in which the slope of T_w varies, decreases as the Grashof number increases, and
- the difference between the wall temperatures corresponding to different values of I_0 are not as important as those in Fig. 6(a).

Fig. 6(b) shows the fully developed non-dimensional temperature profile for $Gr = 7.1 \times 10^7$. As noted previously, the corresponding hydrodynamic regime is laminar for $I_0 = 0.1\%$ and turbulent for $I_0 = 1\%$ and $I_0 = 8\%$. It is therefore not surprising that the temperature profile for $I_0 = 0.1\%$ is very close to the corresponding prediction of the laminar model which

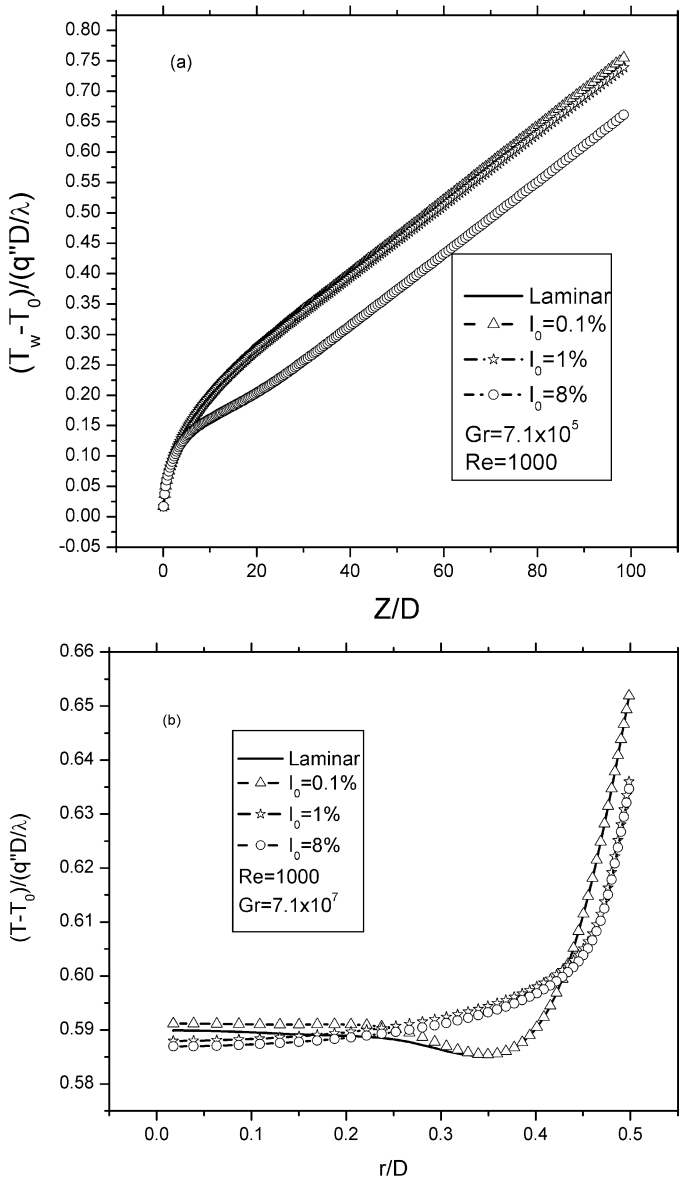

Fig. 6. (a) Axial and (b) radial variation of the fluid temperature.

in turn agrees very well with the analytical solution by Hallman [20]. We note that those two radial temperature profiles exhibit a minimum value at $r/D \cong 0.37$, i.e. at a point where the axial velocity is fairly high (cf. Fig. 4(d)). Thus the thermal energy reaching this point by conduction from the wall and the tube axis is convected downstream by the fast flowing fluid. On the other hand, the temperature profiles for the two turbulent flows ($I_0 = 1\%$ and $I_0 = 8\%$) are also very close. In this case, the temperature decreases monotonically as r/D decreases. The non-dimensional bulk temperature and the heat flux are the same for the four cases depicted in the Fig. 6(b) but, as noted in the discussion of Fig. 6(a), the wall temperature is lower when the flow is turbulent.

4. Conclusion

Mixed convection of air in vertical tubes with uniform wall heat flux was studied with a numerical model based on the steady state three dimensional elliptic conservation equations using both laminar and turbulent formulations. The predicted effects of inlet turbulent intensity on the flow field have been investigated for $Re = 1000$. It was found that the flow regime is influenced by the inlet turbulence intensity and by the Grashof number. Thus, for low Grashof number ($Gr \leqslant 8 \times 10^6$) the fully developed flow is laminar for $I_0 = 0.1\%$ and turbulent for $I_0 = 8\%$. For intermediate Grashof numbers ($Gr = 3 \times 10^7$) the fully developed flow is turbulent for $I_0 \geqslant 0.1\%$ and the laminar model does not converge. Finally, for high Grashof numbers ($Gr = 7.1 \times 10^7$) the fully developed flow is laminar for $I_0 = 0.1\%$ and turbulent for $I_0 \geqslant 1\%$. Thus, for constant low values of I_0 two transitions have been predicted: the first one from laminar to turbulent and the second from turbulent to laminar (relaminarization). The results show that, for certain *Re–Gr* combinations, significant reductions of both the friction coefficient and the wall temperature can be obtained by artificially increasing the turbulent intensity at the tube inlet.

Acknowledgements

The authors thank the University of Sistan and Baluchestan as well as the Natural Science and Engineering Research Council of Canada for their financial support.

References

[1] J.D. Jackson, M.A. Cotton, B.P. Axcell, Studies of mixed convection in vertical tubes, Int. J. Heat Fluid Flow 10 (1989) 2–15.
[2] M. Wang, T. Tsuji, Y. Nagano, Mixed convection with flow reversal in the thermal entrance region of horizontal and vertical pipes, Int. J. Heat Mass Transfer 37 (1994) 2305–2319.
[3] H. Nesreddine, N. Galanis, C.T. Nguyen, Effects of axial diffusion on laminar heat transfer with low Péclet numbers in the entrance region of thin vertical tubes, Numer. Heat Transfer Part A 33 (1998) 247–266.
[4] M. Zghal, N. Galanis, C.T. Nguyen, Developing mixed convection with aiding buoyancy in vertical tubes: a numerical investigation of different flow regimes, Int. J. Therm. Sci. 40 (2001) 816–824.
[5] M.A. Cotton, J.D. Jackson, Vertical tube airflows in the turbulent mixed convection regime calculated using a low-Reynolds-number k–ε model, Int. J. Heat Mass Transfer 33 (1990) 275–286.
[6] S.I. Satake, T. Kunugi, A.M. Shehata, D.M. McEligot, Direct numerical simulation for laminarization of turbulent forced gas flows in circular tubes with strong heating, Int. J. Heat Fluid Flow 21 (2000) 526–534.
[7] H. Tanaka, S. Maruyama, S. Hatano, Combined forced and natural convection heat transfer for upward flow in a uniformly heated vertical pipe, Int. J. Heat Mass Transfer 30 (1987) 165–174.
[8] B. Metais, E.R.G. Eckert, Forced, mixed, and free convection regimes, Trans. ASME J. Heat Transfer 86 (1964) 295–296.
[9] G.F. Scheele, T.J. Hanratty, Effect of natural convection on stability of flow in a vertical pipe, J. Fluid Mech. 14 (1962) 244–256.
[10] Y.C. Su, J.N. Chung, Linear stability analysis of mixed-convection flow in a vertical pipe, J. Fluid Mech. 422 (2000) 141–166.
[11] B. Launder, B.I. Sharma, Application of the energy dissipation model of turbulence to the calculation of flow near a spinning disc, Lett. Heat Mass Transfer 1 (1974) 131–138.
[12] W.P. Jones, B.E. Launder, The calculation of low-Reynolds-number phenomena with a two-equation model of turbulence, Int. J. Heat Mass Transfer 16 (1973) 1119–1129.
[13] A. Behzadmehr, N. Galanis, A. Laneville, Laminar-turbulent transition for low Reynolds number mixed convection in a uniformly heated vertical tube, Int. J. Numer. Methods Heat Fluid Flow 12 (2002) 839–854.

[14] A. Behzadmehr, N. Galanis, A. Laneville, Low Reynolds number mixed convection in vertical tubes with uniform wall heat flux, Int. J. Heat Mass Transfer 46 (2003) 4823–4833.
[15] V.C. Patel, W. Rodi, G. Scheuerer, Turbulence models for near wall and low-Reynolds-number flows, AIAA J. 23 (1985) 1308–1319.
[16] D.P. Mikielewicz, A.M. Shehata, J.D. Jackson, D.M. McEligot, Temperature, velocity and mean turbulence structure in strongly heated internal gas flows. Comparison of numerical predictions with data, Int. J. Heat Mass Transfer 45 (2002) 4333–4352.
[17] B. Zeldin, F.W. Schmidt, Developing flow with combined forced free convection in an isothermal vertical tube, ASME J. Heat Transfer 94 (1972) 211–223.
[18] A.D. Carr, M.A. Connor, H.O. Buhr, Velocity, temperature, and turbulent measurements in air for pipe flow with combined free and forced convection, ASME J. Heat Transfer 95 (1973) 445–452.
[19] FLUENT Documentation, http://www.fluentusers.com/fluent/index.htm.
[20] T.M. Hallman, Combined forced and free-laminar heat transfer in vertical tubes with uniform internal heat generation, ASME J. Heat Transfer (1956) 1831–1841.
[21] M.A. Bernier, B.R. Baliga, Visualization of upward mixed-convection flows in vertical pipes using a thin semitransparent gold-film heater and dye injection, Int. J. Heat Fluid Flow 13 (1992) 241–249.

Further reading

[22] W.B. Hall, J.D. Jackson, Laminarization of a turbulent pipe flow by buoyancy forces, ASME Paper No. 69-HT-55, 1969.